

Photoproduction of Charmonia and Total Charmonium-Proton Cross Sections

J. Hüfner^{a,b}, Yu.P. Ivanov^{a,b,c}, B.Z. Kopeliovich^{b,c} and A.V. Tarasov^{a,b,c}

^a *Institut für Theoretische Physik der Universität, Philosophenweg 19, 69120 Heidelberg, Germany*

^b *Max-Planck Institut für Kernphysik, Postfach 103980, 69029 Heidelberg, Germany*

^c *Joint Institute for Nuclear Research, Dubna, 141980 Moscow Region, Russia*

July 27, 2021

Abstract

Elastic virtual photoproduction cross sections $\gamma^* p \rightarrow J/\psi(\psi') p$ and total charmonium-nucleon cross sections for J/ψ , ψ' and χ states are calculated in a parameter free way with the light-cone dipole formalism and the same input: factorization in impact parameters, light-cone wave functions for the γ^* and the charmonia, and the universal phenomenological dipole cross section which is fitted to other data. The charmonium wave functions are calculated with four known realistic potentials, and two models for the dipole cross section are tested. Very good agreement with data for the cross section of charmonium photoproduction is found in a wide range of s and Q^2 . The inclusion of the Melosh spin rotation increases the ψ' photoproduction rate by a factor 2–3 and removes previously observed discrepancies in the ψ' to J/ψ ratio in photoproduction. We also calculate the charmonium-proton cross sections whose absolute values and energy dependences are found to correlate strongly with the sizes of the states.

1 Introduction

The dynamics of production and interaction of charmonia has drawn attention since their discovery back in 1973. As these heavy mesons have a small size it has been expected that hadronic cross sections may be calculated relying on perturbative QCD. The study of charmonium production became even more intense after charmonium suppression had been suggested as a probe for the creation and interaction of quark-gluon plasma in relativistic heavy ion collisions [1].

Since we will never have direct experimental information on charmonium-nucleon total cross sections one has to extract it from other data for example from elastic photoproduction of charmonia $\gamma p \rightarrow J/\psi(\psi') p$. The widespread believe that one can rely on the vector dominance model (VDM) is based on previous experience the with photoproduction of ρ mesons. However, even a dispersion approach shows that this is quite a risky way, because the J/ψ pole in the complex Q^2 plane is nearly 20 times farther away from the physical region than the ρ pole. The multichannel analysis performed in [2] demonstrates that the corrections are huge, $\sigma_{tot}^{J/\psi p}$ turns out to be more that three times larger than the VDM prediction. Unfortunately, more exact predictions of the multichannel approach, especially for ψ' , need knowledge of many diagonal and off-diagonal amplitudes which are easily summed only if one uses the oversimplified oscillator wave functions and a $q\bar{q}$ -proton cross section of the form $\sigma_{q\bar{q}}(r_T) \propto r_T^2$, where r_T is the transverse $q\bar{q}$ separation.

Instead, one may switch to the quark basis, which should be equivalent to the hadronic basis because of completeness. In this representation the procedure of extracting $\sigma_{tot}^{J/\psi p}$ from photoproduction data cannot be realized directly, but has to be replaced by a different strategy. Namely, as soon as one has expressions for the wave functions of charmonia and the universal dipole cross section $\sigma_{q\bar{q}}(r_T, s)$, one can predict both, the experimentally known charmonium photoproduction cross sections and the unknown $\sigma_{tot}^{J/\psi(\psi') p}$. If the photoproduction data are well described one may have some confidence in the predictions for the $\sigma_{tot}^{J/\psi(\psi') p}$. Of course this procedure will be model dependent, but we believe that this is the

best use of photoproduction data one can presently make. This program was performed for the first time in [3]. The aim of this paper is not to propose a conceptually new scheme, but to calculate within a given approach as accurately as possible and without any free parameters. Wherever there is room for arbitrariness, like forms for the color dipole cross section and those for charmonium wave functions, we use and compare other author's proposals, which have been tested on data different from those used here.

In the light-cone dipole approach the two processes, photoproduction and charmonium-nucleon elastic scattering look as shown in Fig. 1 [3]. The corresponding expressions for the

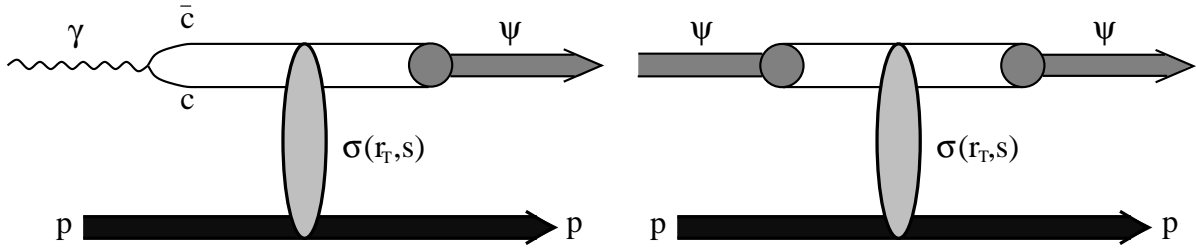


Figure 1: Schematic representation of the amplitudes for the reactions $\gamma^* p \rightarrow \psi p$ (left) and ψp elastic scattering (right) in the rest frame of the proton. The $c\bar{c}$ fluctuation of the photon and the ψ with transverse separation r_T and c.m. energy \sqrt{s} interact with the target proton via the cross section $\sigma(r_T, s)$ and produce a J/ψ or ψ' .

forward amplitudes read

$$\mathcal{M}_{\gamma^* p}(s, Q^2) = \sum_{\mu, \bar{\mu}} \int_0^1 d\alpha \int d^2 \vec{r}_T \Phi_{\psi}^{*(\mu, \bar{\mu})}(\alpha, \vec{r}_T) \sigma_{q\bar{q}}(r_T, s) \Phi_{\gamma^*}^{(\mu, \bar{\mu})}(\alpha, \vec{r}_T, Q^2), \quad (1)$$

$$\mathcal{M}_{\psi p}(s) = \sum_{\mu, \bar{\mu}} \int_0^1 d\alpha \int d^2 \vec{r}_T \Phi_{\psi}^{*(\mu, \bar{\mu})}(\alpha, \vec{r}_T) \sigma_{q\bar{q}}(r_T, s) \Phi_{\psi}^{(\mu, \bar{\mu})}(\alpha, \vec{r}_T). \quad (2)$$

Here the summation runs over spin indexes $\mu, \bar{\mu}$ of the c and \bar{c} quarks, Q^2 is the photon virtuality, $\Phi_{\gamma^*}(\alpha, r_T, Q^2)$ is the light-cone distribution function of the photon for a $c\bar{c}$ fluctuation of separation r_T and relative fraction α of the photon light-cone momentum carried by c or \bar{c} . Correspondingly, $\Phi_{\psi}(\alpha, \vec{r}_T)$ is the light-cone wave function of J/ψ , ψ' and χ (only in Eq. 2). The dipole cross section $\sigma_{q\bar{q}}(r_T, s)$ mediates the transition (*cf* Fig. 1).

In Section 2 we review the status of the factorized light-cone approach to photoproduction of heavy quarkonia. Besides the well known distribution function of quarks in the photon, it needs knowledge of the universal flavor independent dipole cross section which depends on the transverse $\bar{q}q$ separation and energy. In Section 2.1 we introduce two parameterizations available in the literature.

Making use of the nonrelativistic approximation for heavy quarkonia in Section 2.2 we solve the Schrödinger equation with four types of relativistic potentials available in the literature. The next most difficult step is a Lorentz boost to the infinite momentum frame discussed in Section 2.3. Although this procedure is ill defined and no unambiguous recipe is known, we apply the standard and widely used one. We put a special emphasis on importance of the Melosh spin transformation, which turns out to be very important.

The final expression for the photoproduction cross sections is presented in Section 3.1 and results are compared with available data for J/ψ production in Section 3.2. Although the calculations are parameter free they demonstrate a very good agreement with data.

The ratio of ψ' to J/ψ photoproduction yields has drawn attention recently since previous calculations grossly underestimate experimental values. It is demonstrated in Section 3.3 that the Melosh spin transformation which has been overlooked previously, and accompanies the Lorentz boost may be the reason. It has a dramatic impact on the ψ' photoproduction increasing its yield by a factor 2 – 3 in a good agreement with data.

After we will have demonstrated that the approach under discussion quantitatively explains the photoproduction data, we calculate in Section 4 the total charmonium-nucleon cross sections for $J/\psi, \psi'$ and χ -s. We predict quite a steep energy dependence for these cross sections slightly varying for different charmonia. Although the cross sections correlate with the mean charmonium size, this dependence is slower than $\propto \langle r_T^2 \rangle$, and this fact finds a simple explanation. In Section 5 we compare our estimates for charmonium-nucleon cross sections with the effective absorption cross section of charmonium which can be extracted from data on nuclear attenuation of J/ψ and ψ' . Agreement is rather good.

Our results are summarized in Section 6 where we also discuss the physics of energy dependence of the cross sections and the status of our approach. Special attention is given to nuclear attenuation of charmonia which is affected by formation and coherence time phenomena in an important way.

2 Light-cone dipole formalism for virtual photoproduction of charmonia off nucleons

The light cone variable describing longitudinal motion which is invariant to Lorentz boosts is the fraction $\alpha = p_c^+ / p_{\gamma^*}^+$ of the photon light-cone momentum $p_{\gamma^*}^+ = E_{\gamma^*} + p_{\gamma^*}$ carried by the quark or antiquark. In the nonrelativistic approximation (assuming no relative motion of c and \bar{c}) $\alpha = 1/2$ (e.g. [3]), otherwise one should integrate over α (see Eq. (1)). For transversely (T) and longitudinally (L) polarized photons the perturbative photon-quark distribution function in Eq. (1) reads [4, 5],

$$\Phi_{T,L}^{(\mu,\bar{\mu})}(\alpha, \vec{r}_T, Q^2) = \frac{\sqrt{N_c \alpha_{em}}}{2\pi} Z_c \chi_c^{\mu\dagger} \hat{O}_{T,L} \tilde{\chi}_{\bar{c}}^{\bar{\mu}} K_0(\epsilon r_T) , \quad (3)$$

where

$$\tilde{\chi}_{\bar{c}} = i \sigma_y \chi_{\bar{c}}^* ; \quad (4)$$

χ and $\bar{\chi}$ are the spinors of the c -quark and antiquark respectively; $Z_c = 2/3$. $K_0(\epsilon r_T)$ is the modified Bessel function with

$$\epsilon^2 = \alpha(1 - \alpha)Q^2 + m_c^2 . \quad (5)$$

The operators $\hat{O}_{T,L}$ have the form:

$$\hat{O}_T = m_c \vec{\sigma} \cdot \vec{e}_\gamma + i(1 - 2\alpha) (\vec{\sigma} \cdot \vec{n}) (\vec{e}_\gamma \cdot \vec{\nabla}_{r_T}) + (\vec{n} \times \vec{e}_\gamma) \cdot \vec{\nabla}_{r_T} , \quad (6)$$

$$\hat{O}_L = 2Q\alpha(1 - \alpha) \vec{\sigma} \cdot \vec{n} , \quad (7)$$

where $\vec{n} = \vec{p}/p$ is a unit vector parallel to the photon momentum and \vec{e} is the polarization vector of the photon. Effects of the non-perturbative interaction within the $q\bar{q}$ fluctuation are negligible for the heavy charmed quarks.

The color dipole cross section $\sigma_{q\bar{q}}(r_T, s)$ is poorly known from first principles. It is expected to vanish $\propto r_T^2$ at small $r_T \rightarrow 0$ due to color screening [6] and to level off at large separations due to a finite range of gluon propagation. We employ phenomenological approaches described in section 2.1.

The charmonium wave function is well defined in the rest frame where one can rely on the Schrödinger equation. We present solutions for four potentials proposed in the literature (section 2.2). As soon as the rest frame wave function is known, one may be tempted to apply the Lorentz transformation to the $c\bar{c}$ pair as it would be a classical system and boost it to the infinite momentum frame. However, quantum effects are important and in the infinite momentum frame a series of different Fock states emerges from the Lorentz boost. (Compare with a Lorentz boost of a positronium: Weizsäcker-Williams photons appear.) Therefore the lowest $|c\bar{c}\rangle$ component in the infinite momentum frame does not represent the $|c\bar{c}\rangle$ in the rest frame. We rely on the widely used procedure for the generation of the light-cone wave functions of charmonia and describe it in section 2.3.

2.1 Phenomenological dipole cross section

The dipole formalism for hadronic interactions introduced in [6] expands the hadronic cross section over the eigen states of the interaction which in QCD are the dipoles with a definite transverse separation (see (1)). Correspondingly, the values of the dipole cross section $\sigma_{q\bar{q}}(r_T)$ for different r_T are the eigenvalues of the elastic amplitude operator. This cross section is flavor invariant, due to universality of the QCD coupling, and vanishes like $\sigma_{q\bar{q}}(r_T) \propto r_T^2$ for $r_T \rightarrow 0$. The latter property is sometimes referred to as color transparency.

The total cross sections for all hadrons and (virtual) photons are known to rise with energy. Apparently, the energy dependence cannot originate from the hadronic wave functions in Eqs. (1, 2), but only from the dipole cross section. In the approximation of two-gluon exchange used in [6] the dipole cross section is constant, the energy dependence originates from higher order corrections related to gluon radiation. On the other way, one can stay

with two-gluon exchange, but involve higher Fock states which contain gluons in addition to the $q\bar{q}$. Both approaches correspond to the same set of Feynman graphs. We prefer to introduce energy dependence into $\sigma_{q\bar{q}}(r_T, s)$ and not include higher Fock states into the wave functions.

For small size dipoles essential for DIS one may apply perturbative QCD and the energy dependence comes as an effect of gluon radiation treated in the leading-log($1/x$) approximation [7, 8]. In the opposite limit of large separations typical for light hadrons one can also calculate the effects of gluon bremsstrahlung making use of smallness of the quark-gluon correlation radius [9].

However, the intermediate case we are interested in, is the most complicated one as usual. No reliable way to sum up higher order corrections is known so far. Therefore we use a phenomenological form which interpolates between the two limiting cases of small and large separations. Few parameterizations are available in the literature, we choose two of them which are simple, but quite successful in describing data and denote them by the initials of the authors as “GBW” [10] and “KST” [11].

We have

$$\begin{aligned} \text{“GBW”}: \quad \sigma_{q\bar{q}}(r_T, x) &= 23.03 \left[1 - e^{-r_T^2/r_0^2(x)} \right] \text{ mb} , \\ r_0(x) &= 0.4 \left(\frac{x}{x_0} \right)^{0.144} \text{ fm} , \end{aligned} \tag{8}$$

where $x_0 = 3.04 \cdot 10^{-4}$. The proton structure function calculated with this parameterization fits very well all available data at small x and for a wide range of Q^2 [10]. However, it obviously fails describing the hadronic total cross sections, since it never exceeds the value 23.03 mb. The x -dependence guarantees Bjorken scaling for DIS at high Q^2 , however, Bjorken x is not a well defined quantity in the soft limit. Instead we use the prescription of [12], $x = (M_\psi^2 + Q^2)/s$, where M_ψ is the charmonium mass.

This problem as well as the difficulty with the definition of x have been fixed in [11]. The dipole cross section is treated as a function of the c.m. energy \sqrt{s} , rather than x , since \sqrt{s} is more appropriate for hadronic processes. A similarly simple form for the dipole cross

section is used

$$\text{“KST”}: \quad \sigma_{\bar{q}q}(r_T, s) = \sigma_0(s) \left[1 - e^{-r_T^2/r_0^2(s)} \right]. \quad (9)$$

The values and energy dependence of hadronic cross sections is guaranteed by the choice of

$$\sigma_0(s) = 23.6 \left(\frac{s}{s_0} \right)^{0.08} \left(1 + \frac{3 r_0^2(s)}{8 \langle r_{ch}^2 \rangle} \right) \text{ mb}, \quad (10)$$

$$r_0(s) = 0.88 \left(\frac{s}{s_0} \right)^{-0.14} \text{ fm}. \quad (11)$$

The energy dependent radius $r_0(s)$ is fitted to data for the proton structure function $F_2^p(x, Q^2)$, $s_0 = 1000 \text{ GeV}^2$ and the mean square of the pion charge radius $\langle r_{ch}^2 \rangle = 0.44 \text{ fm}^2$. The improvement at large separations leads to a somewhat worse description of the proton structure function at large Q^2 . Apparently, the cross section dependent on energy, rather than x , cannot provide Bjorken scaling. Indeed, parameterization (9) is successful only up to $Q^2 \approx 10 \text{ GeV}^2$.

In fact, the cases we are interested in, charmonium production and interaction, are just in between the regions where either of these parameterization is successful. Therefore, we suppose that the difference between predictions using Eq. (8) and (9) is a measure of the theoretical uncertainty which fortunately turns out to be rather small.

We demonstrate in Fig. 2 a few examples of r_T^2 -dependence of the dipole cross section at different energies for both parameterization. The KST cross section reveals a nontrivial behavior, it rises with energy at $r_T < 3 \text{ fm}^2$, but decreases at larger separations. This is however a temporary effect, $\sigma_0(s)$ reaches minimum at $\sqrt{s} \approx 77 \text{ GeV}$ and then slowly rises at higher energies. Such a peculiar behavior is a consequence of our original intention to reproduce the energy dependence of the hadronic cross sections $\sigma_{tot}^{hp} \propto s^{0.08}$ keeping the form (9) of the cross section. Of course data are insensitive to the cross section at such large separations.

Both GBW and KST cross section vanish $\propto r_T^2$ at small r_T , however considerably deviate from this simple behavior at large separations. Quite often, the simplest parameterization

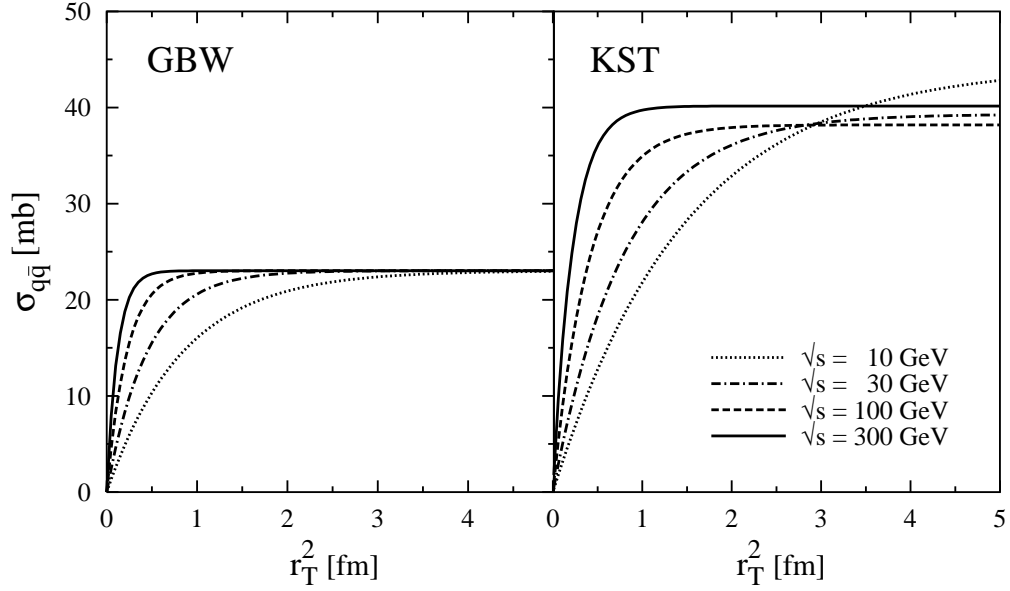


Figure 2: The dipole cross section as function of r_T^2 at energies $\sqrt{s} = 10, 30, 100$ and 300 GeV for GBW (left) and KST (right) parameterizations.

($\propto r_T^2$) for the dipole cross section is used. For the coefficient in front of r_T^2 we employ the expression obtained by the first term of Taylor expansion of Eq. (9):

$$\text{“}r_T^2\text{”}: \quad \sigma_{q\bar{q}}(r_T, s) = \frac{\sigma_0(s)}{r_0^2(s)} \cdot r_T^2. \quad (12)$$

2.2 Charmonium wave functions

The spatial part of the $c\bar{c}$ pair wave function satisfying the Schrödinger equation

$$\left(-\frac{\Delta}{m_c} + V(r) \right) \Psi_{nlm}(\vec{r}) = E_{nl} \Psi_{nlm}(\vec{r}) \quad (13)$$

is represented in the form

$$\Psi(\vec{r}) = \Psi_{nl}(r) \cdot Y_{lm}(\theta, \varphi), \quad (14)$$

where \vec{r} is 3-dimensional $c\bar{c}$ separation, $\Psi_{nl}(r)$ and $Y_{lm}(\theta, \varphi)$ are the radial and orbital parts of the wave function. The equation for radial $\Psi(r)$ is solved with the help of the program [13]. The following four potentials $V(r)$ have been used (see Fig. 3):

- “COR”: Cornell potential [15],

$$V(r) = -\frac{k}{r} + \frac{r}{a^2} \quad (15)$$

with $k = 0.52$, $a = 2.34 \text{ GeV}^{-1}$ and $m_c = 1.84 \text{ GeV}$.

- “BT”: Potential suggested by Buchmüller and Tye [14] with $m_c = 1.48 \text{ GeV}$. It has a similar structure as the Cornell potential: linear string potential at large separations and Coulomb shape at short distances with some refinements, however.

- “LOG”: Logarithmic potential [16]

$$V(r) = -0.6635 \text{ GeV} + (0.733 \text{ GeV}) \log(r \cdot 1 \text{ GeV}) \quad (16)$$

with $m_c = 1.5 \text{ GeV}$.

- “POW”: Power-law potential [17]

$$V(r) = -8.064 \text{ GeV} + (6.898 \text{ GeV})(r \cdot 1 \text{ GeV})^{0.1} \quad (17)$$

with $m_c = 1.8 \text{ GeV}$.

The shapes of the four potentials is displayed in Fig. 3 and differ from each other only at large r ($\geq 1 \text{ fm}$) and very small r ($\leq 0.05 \text{ fm}$) separations. Note, however, that COR and POW use $m_c \approx 1.8 \text{ GeV}$, while BT and LOG use $m_c \approx 1.5 \text{ GeV}$ for the mass of the charmed quark. This difference will have significant consequences.

The results of calculations for the radial part $\Psi_{nl}(r)$ of the $1S$ and $2S$ states are depicted in Fig. 4. For the ground state all the potentials provide a very similar behavior for $r > 0.3 \text{ fm}$, while for small r the predictions are differ by up to 30%. The peculiar property of the $2S$ state wave function is the node at $r \approx 0.4 \text{ fm}$ which causes strong cancelations in the matrix elements Eq. (1) and as a result, a suppression of photoproduction of ψ' relative to J/ψ [3, 18].

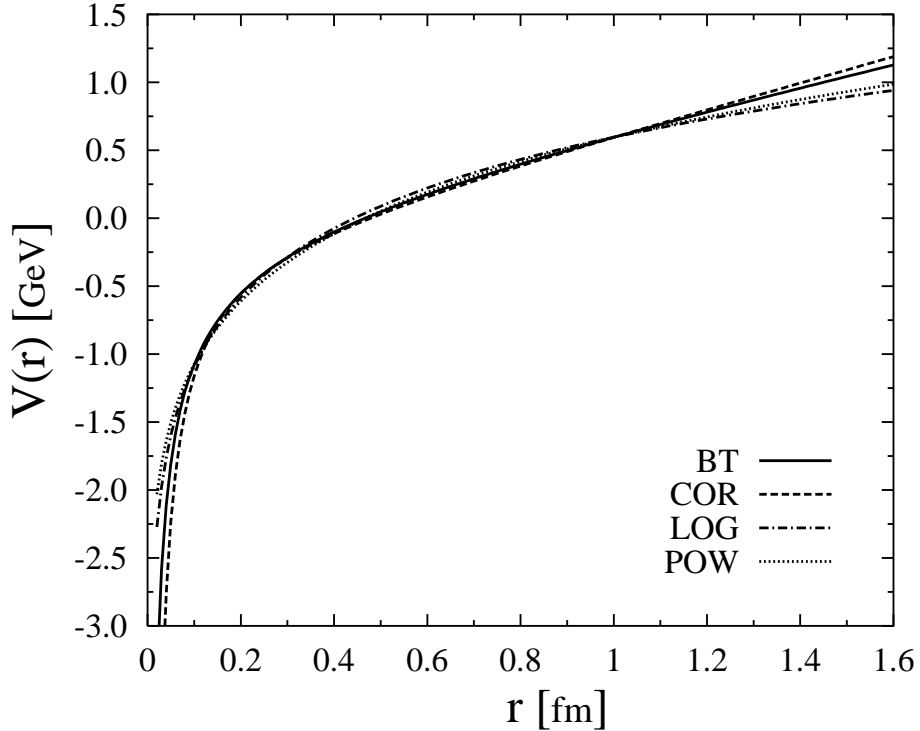


Figure 3: *Shapes of the potentials $V(r)$ for the four parameterizations employed in this paper. The curves for COR, LOG and POW are normalized at $r = 1$ fm to the value of BT potential.*

2.3 Light-cone wave functions for the bound states

As has been mentioned, the lowest Fock component $|c\bar{c}\rangle$ in the infinite momentum frame is not related by simple Lorentz boost to the wave function of charmonium in the rest frame. This makes the problem of building the light-cone wave function for the lowest $|c\bar{c}\rangle$ component difficult, no unambiguous solution is yet known. There are only recipes in the literature, a simple one widely used [19], is the following. One applies a Fourier transformation from coordinate to momentum space to the known spatial part of the non-relativistic wave function (14), $\Psi(\vec{r}) \Rightarrow \Psi(\vec{p})$, which can be written as a function of the effective mass of the $c\bar{c}$, $M^2 = 4(p^2 + m_c^2)$, expressed in terms of light-cone variables

$$M^2(\alpha, p_T) = \frac{p_T^2 + m_c^2}{\alpha(1 - \alpha)}. \quad (18)$$

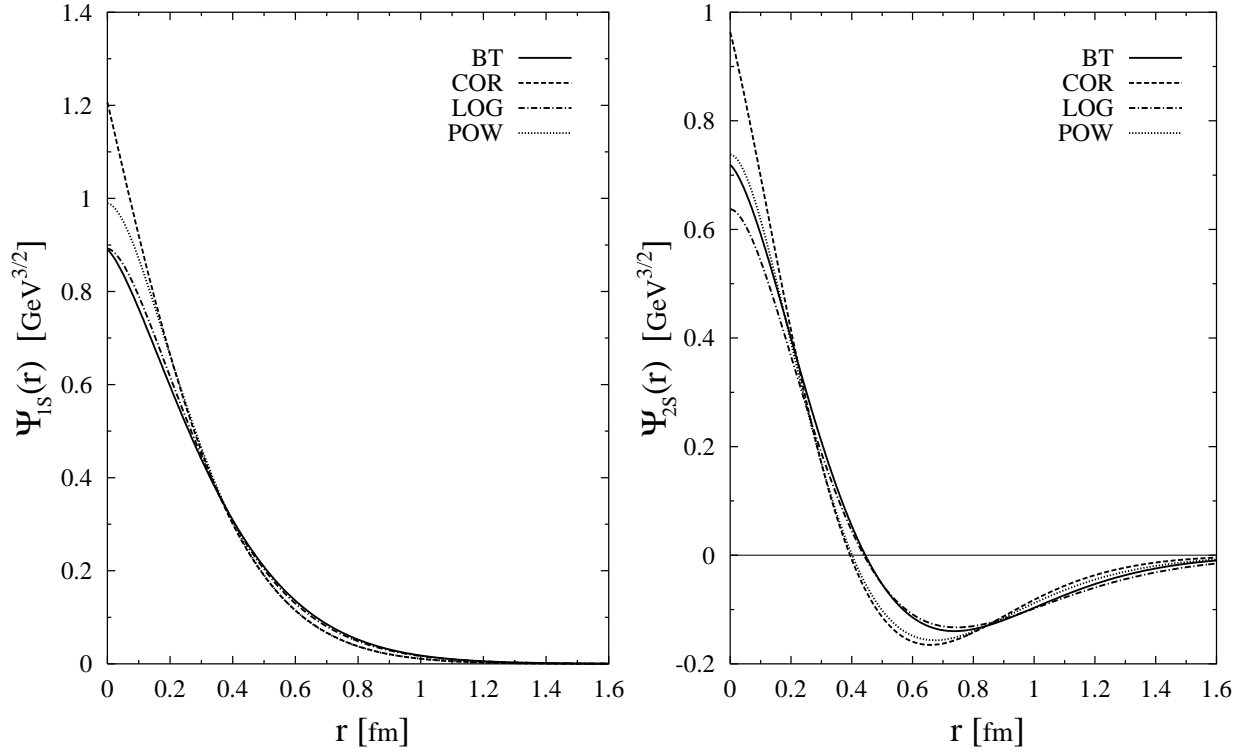


Figure 4: The radial part of the wave function $\Psi_{nl}(r)$ for the $1S$ and $2S$ states calculated with four different potentials (see text).

In order to change integration variable p_L to the light-cone variable α one relates them via M , namely $p_L = (\alpha - 1/2)M(p_T, \alpha)$. In this way the $c\bar{c}$ wave function acquires a kinematical factor

$$\Psi(\vec{p}) \Rightarrow \sqrt{2} \frac{(p^2 + m_c^2)^{3/4}}{(p_T^2 + m_c^2)^{1/2}} \cdot \Psi(\alpha, \vec{p}_T) \equiv \Phi_\psi(\alpha, \vec{p}_T) . \quad (19)$$

This procedure is used in [20] and the result is applied to calculation of the amplitudes (1). The result is discouraging, since the ψ' to J/ψ ratio of the photoproduction cross sections are far too low in comparison with data. However, the oversimplified dipole cross section $\sigma_{q\bar{q}}(r_T) \propto r_T^2$ has been used, and what is even more essential, the important ingredient of Lorentz transformations, the Melosh spin rotation, has been left out. The spin transformation has also been left out in the recent publication [21] which repeats the calculations of [20] with a more realistic dipole cross section which levels off at large separations. This leads to suppression of the node-effect (less cancelation) and enhancement of Ψ' photoproduction.

Nevertheless, the calculated ψ' to J/ψ ratio is smaller than the data by a factor of two.

The 2-dimensional spinors χ_c and $\chi_{\bar{c}}$ describing c and \bar{c} respectively in the infinite momentum frame are known to be related via the Melosh rotation [22, 19] to the spinors $\bar{\chi}_c$ and $\bar{\chi}_{\bar{c}}$ in the rest frame:

$$\begin{aligned}\bar{\chi}_c &= \hat{R}(\alpha, \vec{p}_T) \chi_c , \\ \bar{\chi}_{\bar{c}} &= \hat{R}(1 - \alpha, -\vec{p}_T) \chi_{\bar{c}} ,\end{aligned}\tag{20}$$

where the matrix $R(\alpha, \vec{p}_T)$ has the form:

$$\hat{R}(\alpha, \vec{p}_T) = \frac{m_c + \alpha M - i [\vec{\sigma} \times \vec{n}] \vec{p}_T}{\sqrt{(m_c + \alpha M)^2 + p_T^2}} .\tag{21}$$

Since the potentials we use in section 2.2 contain no spin-orbit term, the $c\bar{c}$ pair is in S -wave. In this case spatial and spin dependences in the wave function factorize and we arrive at the following light cone wave function of the $c\bar{c}$ in the infinite momentum frame

$$\Phi_{\psi}^{(\mu, \bar{\mu})}(\alpha, \vec{p}_T) = U^{(\mu, \bar{\mu})}(\alpha, \vec{p}_T) \cdot \Phi_{\psi}(\alpha, \vec{p}_T) ,\tag{22}$$

where

$$U^{(\mu, \bar{\mu})}(\alpha, \vec{p}_T) = \chi_c^{\mu\dagger} \hat{R}^\dagger(\alpha, \vec{p}_T) \vec{\sigma} \cdot \vec{e}_\psi \sigma_y \hat{R}^*(1 - \alpha, -\vec{p}_T) \sigma_y^{-1} \tilde{\chi}_{\bar{c}}^{\bar{\mu}}\tag{23}$$

and $\tilde{\chi}_{\bar{c}}$ is defined in (4).

Note that the wave function (22) is different from one used in [23, 24, 25] where it was assumed that the vertex $\psi \rightarrow c\bar{c}$ has the structure $\psi_\mu \bar{u} \gamma_\mu u$ like the for the photon $\gamma^* \rightarrow c\bar{c}$. The rest frame wave function corresponding to such a vertex contains S wave and D wave. The weight of the latter is dictated by the structure of the vertex and cannot be justified by any reasonable nonrelativistic potential model for the $c\bar{c}$ interaction.

Now we can determine the light-cone wave function in the mixed longitudinal momentum - transverse coordinate representation:

$$\Phi_{\psi}^{(\mu, \bar{\mu})}(\alpha, \vec{r}_T) = \frac{1}{2\pi} \int d^2 \vec{p}_T e^{-i\vec{p}_T \vec{r}_T} \Phi_{\psi}^{(\mu, \bar{\mu})}(\alpha, \vec{p}_T) .\tag{24}$$

The spatial component $\Phi_\psi(\alpha, \vec{r}_T)$ of Eq. (19) in mixed representation (24) is plotted as a function of r_T and α in Fig. 5 for $J/\psi(1S)$ and $\psi'(2S)$ states. While the $1S$ wave function depends monotonically on r_T and smoothly vanishes at small α , the wave function of the $2S$ state demonstrates a nontrivial behavior: the node disappears for small α .

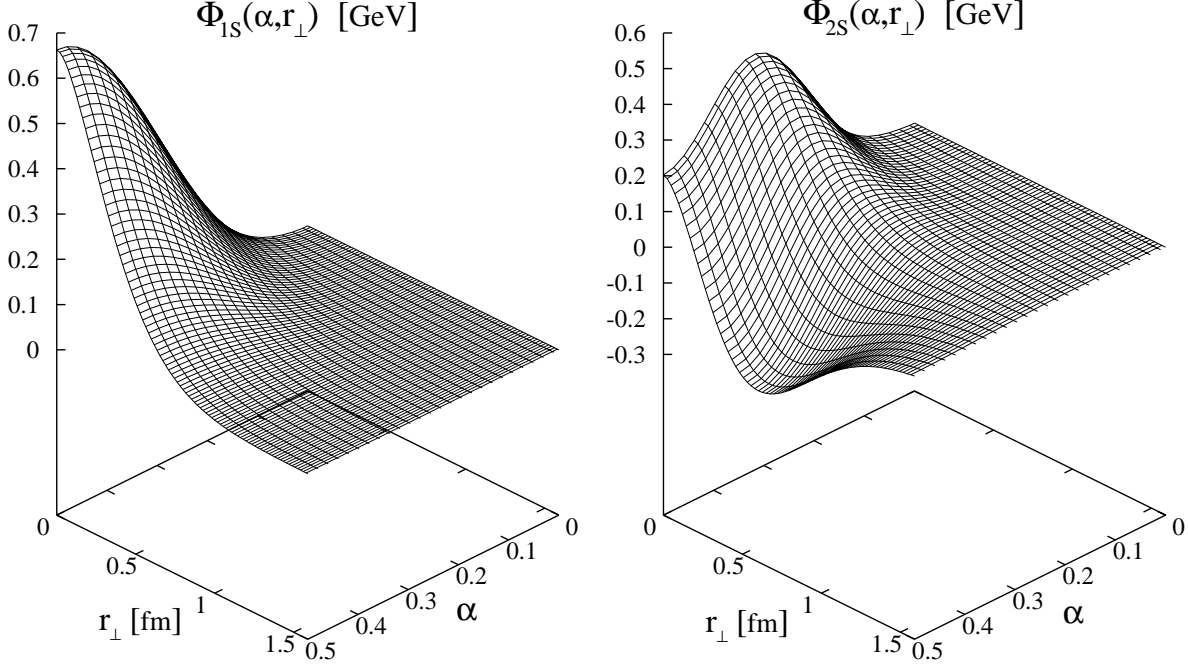


Figure 5: Three-dimensional plot for the light-cone wave functions for $J/\psi(1S)$ and $\psi'(2S)$ in the mixed $\alpha - \vec{r}_T$ representation for the BT potential [14].

3 Calculations and comparison with data

3.1 The final expressions

Having the light-cone wave function of charmonium in momentum representation Eq. (22) it is more convenient to switch to an integration over \vec{p}_T in the matrix element Eq. (1):

$$\mathcal{M}_{T,L}(s, Q^2) = \int_0^1 d\alpha \int d^2\vec{p}_T \Phi_\psi^*(\alpha, \vec{p}_T) \Sigma_{T,L}(\alpha, \vec{p}_T, s, Q^2) , \quad (25)$$

where

$$\Sigma_{T,L}(\alpha, \vec{p}_T, s, Q^2) = \frac{1}{2\pi} \sum_{\mu, \bar{\mu}} U^{(\mu, \bar{\mu})}(\alpha, \vec{p}_T) \int d^2 \vec{r}_T e^{i \vec{p}_T \vec{r}_T} \sigma(r_T, s) \Phi_{T,L}^{(\mu, \bar{\mu})}(\alpha, \vec{r}_T) . \quad (26)$$

If the dipole cross section depends on r_T like $\sigma_0(1 - e^{-r_T^2/r_0^2})$ (see Eqs. (8) and (9)), then $\Sigma(\alpha, \vec{p}_T, s, Q^2)$ which includes the effects of spin rotation, can be expressed as follows:

$$\begin{aligned} \Sigma_T(\alpha, \vec{p}_T, s, Q^2) &= \frac{1}{m_c} \left[m_T - \frac{2 p_T^2 \alpha (1 - \alpha)}{m_T + m_L} \right] \tilde{\Sigma}_T(\alpha, \vec{p}_T, s, Q^2) \\ &\quad - \frac{2 p_T^2}{m_q m_T r_0^2} \left[1 + \frac{m_T (1 - 2\alpha)}{m_T + m_L} \right] \frac{\partial \tilde{\Sigma}_t(\alpha, \vec{p}_T, s, Q^2)}{\partial p_T^2} , \end{aligned} \quad (27)$$

$$\Sigma_L(\alpha, \vec{p}_T, s, Q^2) = \frac{m_q^2 + m_T m_L}{m_c (m_T + m_L)} \tilde{\Sigma}_L(\alpha, \vec{p}_T, s, Q^2) , \quad (28)$$

where $m_T^2 = m_c^2 + p_T^2$, $m_L^2 = 4 m_c^2 \alpha (1 - \alpha)$ and

$$\tilde{\Sigma}_{T,L}(\alpha, \vec{p}_T, s, Q^2) = \frac{\sigma_0(s)}{2\pi} \int d^2 r_T e^{i \vec{p}_T \vec{r}_T} \Phi_{T,L}(\alpha, \vec{r}_T, Q^2) \cdot [1 - e^{-r_T^2/r_0^2(s)}] , \quad (29)$$

$$\tilde{\Sigma}_t(\alpha, \vec{p}_T, s, Q^2) = \frac{\sigma_0(s)}{2\pi} \int d^2 r_T e^{i \vec{p}_T \vec{r}_T} \Phi_T(\alpha, \vec{r}_T, Q^2) \cdot e^{-r_T^2/r_0^2(s)} , \quad (30)$$

$$\Phi_T(\alpha, r_T, Q^2) = \frac{1}{\pi} \sqrt{\frac{2\alpha_{em}}{3}} m_q K_0(\epsilon r_T) , \quad (31)$$

$$\Phi_L(\alpha, r_T, Q^2) = \frac{2}{\pi} \sqrt{\frac{\alpha_{em}}{3}} Q \alpha (1 - \alpha) K_0(\epsilon r_T) . \quad (32)$$

The photoproduction cross section is given by

$$\sigma_{\gamma^* p \rightarrow \psi p}(s, Q^2) = \frac{|\tilde{\mathcal{M}}_T(s, Q^2)|^2 + \varepsilon |\tilde{\mathcal{M}}_L(s, Q^2)|^2}{16 \pi B} , \quad (33)$$

where ε is the photon polarization (for H1 data $\langle \varepsilon \rangle = 0.99$); B is the slope parameter in reaction $\gamma^* p \rightarrow \psi p$. We use the experimental value [29] $B = 4.73 \text{ GeV}^{-2}$. $\tilde{\mathcal{M}}_{T,L}$ includes also the correction for the real part of the amplitude:

$$\tilde{\mathcal{M}}_{T,L}(s, Q^2) = \mathcal{M}_{T,L}(s, Q^2) \left(1 - i \frac{\pi}{2} \frac{\partial \ln \mathcal{M}_{T,L}(s, Q^2)}{\partial \ln s} \right) , \quad (34)$$

where we apply the well known derivative analyticity relation between the real and imaginary parts of the forward elastic amplitude [26]. The correction from the real part is not small since the cross section of charmonium photoproduction is a rather steep function of energy (see below).

3.2 s and Q^2 dependence of $\sigma(\gamma^*p \rightarrow J/\psi p)$

Now we are in a position now to calculate the cross section of charmonium photoproduction using Eq. (33). The results for J/ψ are compared with the data in Fig. 6. Calculations are performed with GBW and KST parameterizations for the dipole cross section and for wave functions of the J/ψ calculated from BT, LOG, COR and POW potentials. One observes

- There are no major differences for the results using the GBW and KST parameterizations.
- The use of different potentials to generate the wave functions of the J/ψ leads to two distinctly different behaviors. The potentials labeled BT and LOG (see sect. 2.2) describe the data very well, while the potentials COR and LOG underestimate them by a factor of two. The different behavior has been traced to the following origin: BT and LOG use $m_c \approx 1.5 \text{ GeV}$, but COR and POW $m_c \approx 1.8 \text{ GeV}$. While the bound state wave functions of J/ψ are little affected by this difference (see Fig. 4), the photon wave function Eq. (3) depends sensitively on m_c via the argument Eq. (5) of the K_0 function.

We compare our calculations also with data for the Q^2 dependence of the cross section. The data are plotted in Fig. 7 at c.m. energy $\sqrt{s} = 90 \text{ GeV}$ as a function of $Q^2 + M_{J/\psi}^2$, since in this form both, data and calculations display an approximate power law dependence. Such a dependence on $Q^2 + M_{J/\psi}^2$ is suggested by the variable ϵ^2 in Eq. (5), which for $\alpha = 1/2$ takes the value $Q^2 + (2m_c)^2$. It may be considered as an indication that $\alpha = 1/2$ is a reasonable approximation for the nonrelativistic charmonium wave function.

Our results are depicted for BT and COR potentials and using GBW and KST cross sections. Agreement with the calculations based on BT potential is again quite good, while the COR potential grossly underestimate the data at small Q^2 . Although the GBW and KST dipole cross sections lead to nearly the same cross sections for real photoproduction, their predictions at high Q^2 are different by a factor 2–3. Supposedly the GBW parameterization

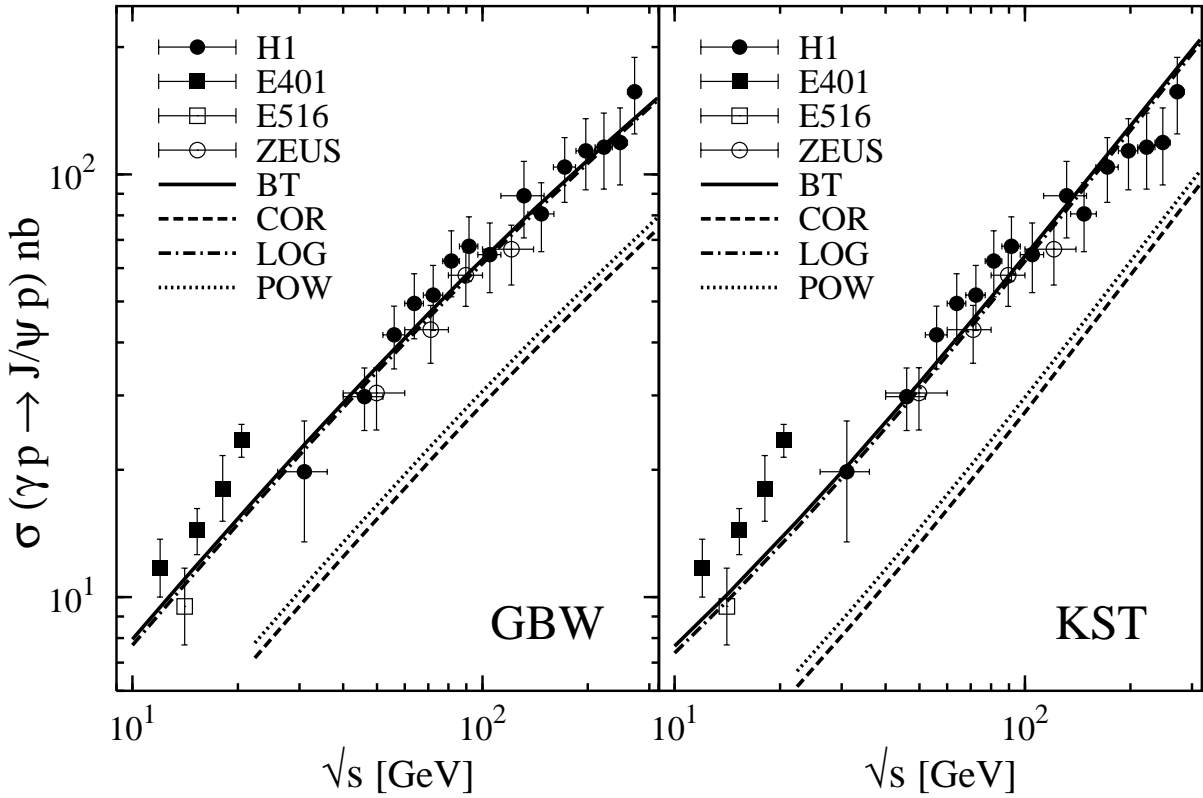


Figure 6: Integrated cross section for elastic photoproduction $\gamma p \rightarrow J/\psi p$ with real photons ($Q^2 = 0$) as a function of the energy calculated with GBW and KST dipole cross sections and for four potentials to generate J/ψ wave functions. Experimental data points from the H1 [29], E401 [32], E516 [33] and ZEUS [30] experiments.

should be more trustable at $Q^2 \gg M_\Psi^2$.

3.3 Importance of spin effects for the ψ' to J/ψ ratio

It turns out that the effects of spin rotation have a gross impact on the cross section of elastic photoproduction $\gamma p \rightarrow J/\psi(\psi)p$. To demonstrate these effects we present the results of our calculations at $\sqrt{s} = 90 \text{ GeV}$ in Table 1. The upper half of the table shows the photoproduction cross sections for J/ψ for different parameterizations of the dipole cross section (GBW, KST, “ r_T^2 ”) and potentials (BT, COR, LOG, POW). The numbers in parenthesis show what the cross section would be, if the spin rotation effects were neglected. We see

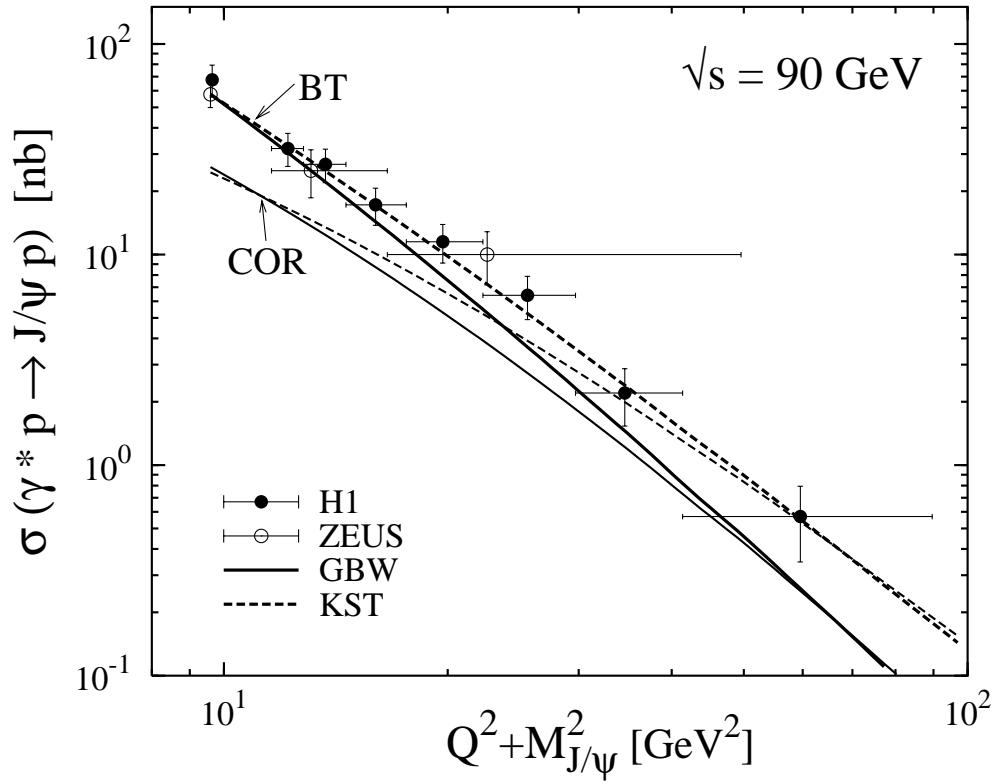


Figure 7: Integrated cross section for elastic photo production as a function of the photon virtuality $Q^2 + M_{J/\psi}^2$ at energy $\sqrt{s} = 90$ GeV. Solid and dashed curves are calculated with GBW and KST dipole cross sections, while thick and thin curves correspond to BT and COR potentials, respectively. Results obtained with LOG and POW potentials are very close to that curves (LOG similar to BT and POW to COR, see also Fig. 6).

that these effects add 30-40% to the J/ψ photoproduction cross section.

The spin rotation effects turn out to have a much more dramatic impact on ψ' increasing the photoproduction cross section by a factor 2-3. This is visible in the lower half of the table which shows the ratio $R = \sigma(\psi')/\sigma(J/\psi)$ of photoproduction cross sections, where the number in parenthesis correspond to no spin rotation effects included. This spin effects explain the large values of the ratio R observed experimentally. Our results for R are about twice as large as evaluated in [21] and even more than in [20].

The ratio of ψ' to J/ψ photoproduction cross sections is depicted as function of c.m.

Table 1: The photoproduction $\gamma p \rightarrow J/\psi p$ cross-section $\sigma(J/\psi)$ in nb and the ratio $R = \sigma(\psi')/\sigma(J/\psi)$ for the four different types of potentials (BT, LOG, COR, POW) and the three parameterizations (GBW, KST, r_T^2) for the dipole cross section $\sigma(r_T, s)$ at $\sqrt{s} = 90$ GeV. The values in parentheses correspond to the case when the spin rotation is neglected.

		BT	LOG	COR	POW
$\boxed{\sigma}$	GBW	52.01 (37.77)	50.78 (36.63)	23.13 (17.07)	24.94 (18.64)
	KST	49.96 (35.87)	48.49 (34.57)	21.05 (15.42)	22.83 (16.92)
	r_T^2	66.67 (47.00)	64.07 (44.86)	25.81 (18.71)	28.23 (20.66)
\boxed{R}	GBW	0.147 (0.075)	0.117 (0.060)	0.168 (0.099)	0.144 (0.085)
	KST	0.147 (0.068)	0.118 (0.054)	0.178 (0.099)	0.152 (0.084)
	r_T^2	0.101 (0.034)	0.081 (0.027)	0.144 (0.070)	0.121 (0.058)

energy in Fig. 8 and as a function of Q^2 in Fig. 9 for all four potentials and for the parameterizations of the dipole cross sections GBW and KST.

Our calculations agree with available data, but error bars are too large to provide a more precise test for the theory. Remarkably, the ratio $R(s)$ rises with energy. This result is in variance with the naive expectation based on the larger size of the ψ' and on the usual rule: the smaller the size of the $q\bar{q}$ dipole, the steeper its energy dependence. There is, however, no contradiction, since this is another manifestation of the node in the wave function of ψ' . Indeed, as function of energy mostly the short distance part of the dipole cross section $\sigma_{q\bar{q}}(r_T)$ rises. It enhances the positive contribution for distances shorter than the node position in the ψ' wave function. Therefore, with increasing energy the cancelation in the amplitude of ψ' production is reduced. This effect leads to a steeper energy dependence of ψ' production compared to J/ψ . The effect is stronger for GBW than KST parameterizations, since the

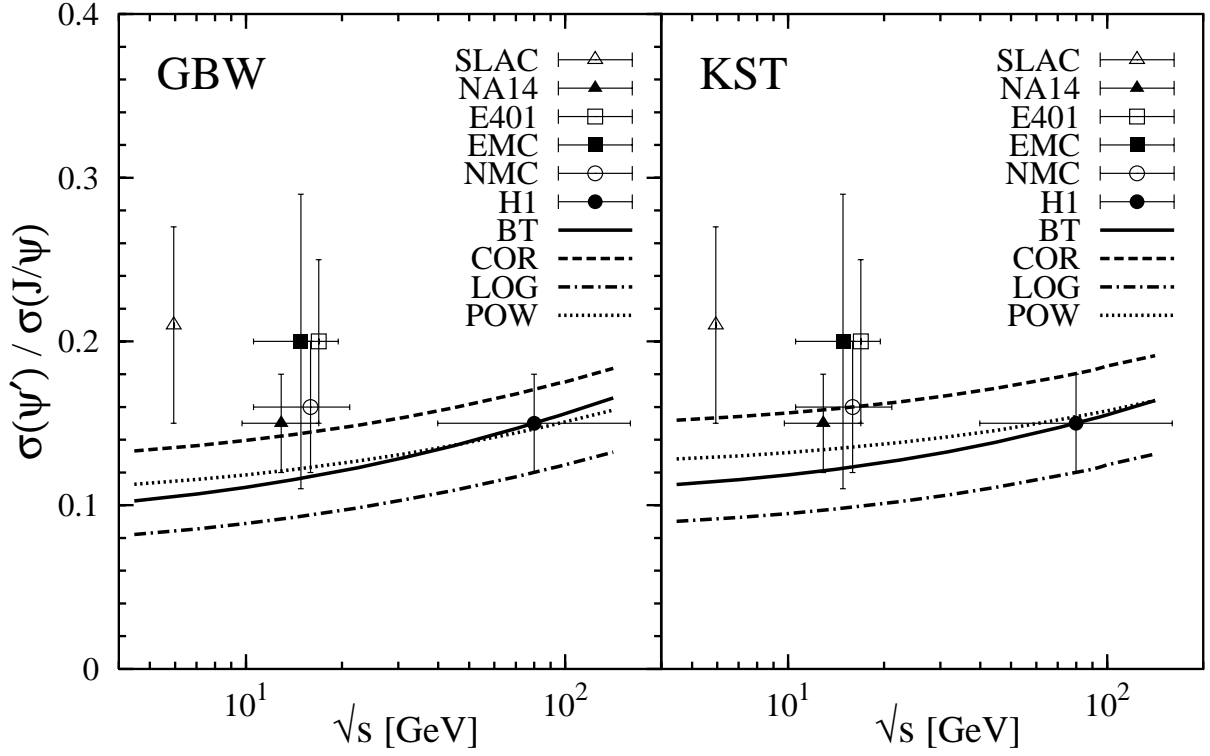


Figure 8: The ratio of ψ' to J/ψ photoproduction cross sections as a function of c.m. energy calculated for all four potentials with GBW and KST parameterizations for the dipole cross section. Experimental data points from the SLAC [34], NA14 [35], E401 [36], EMC [37], NMC [38] and H1 [27] experiments.

GBW cross section does not rise with energy at all at large separations. Note that this situation is specific for photoproduction because the nodeless wave function of the photon is projected to the sign changing wave function of ψ' . This should not happen in the case of elastic $J/\psi(\Psi')$ - p scattering (see below).

Similarly of the node effect leads to a rising Q^2 -dependence of the ψ' to J/ψ ratio in the photoproduction cross sections. Our calculations are compared with available data in Fig. 9 for the GBW and KST parameterizations respectively.

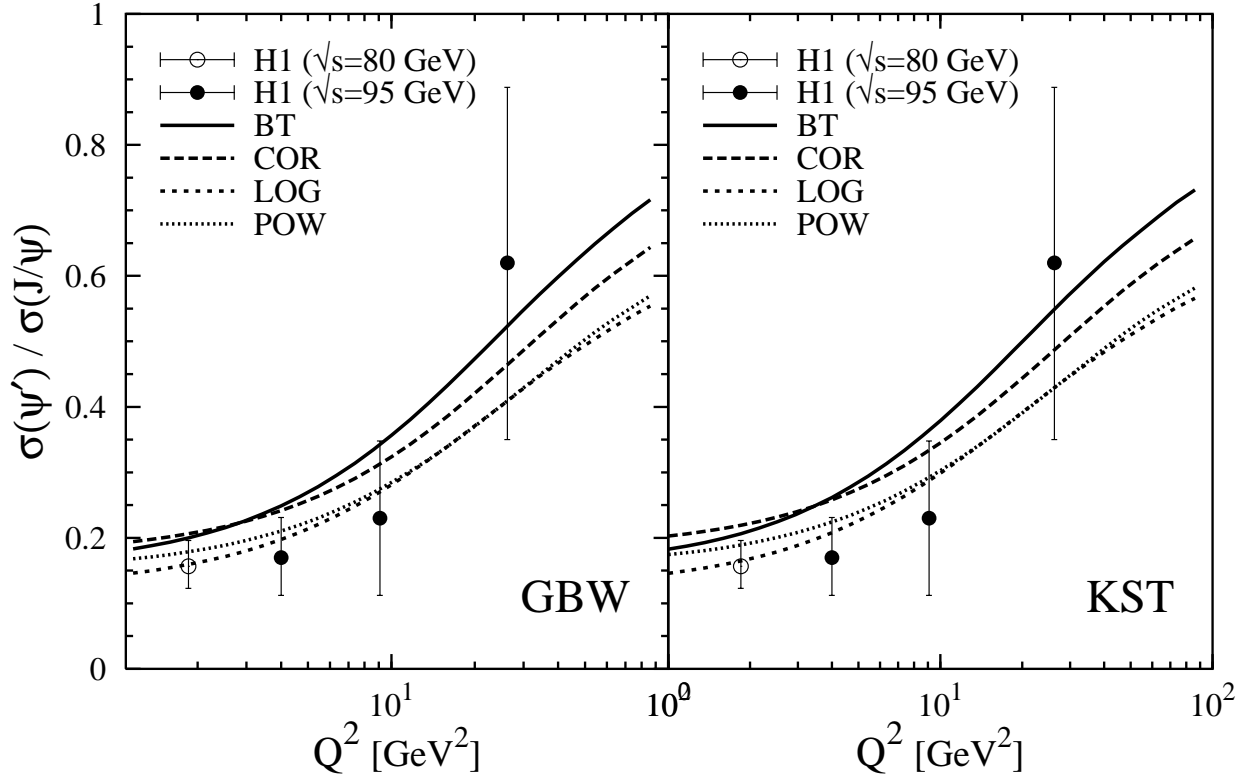


Figure 9: The ratio of ψ' to J/ψ photoproduction cross sections as a function of the photon virtuality Q^2 at energy $\sqrt{s} = 90$ GeV all four potentials with GBW and KST parameterizations for the dipole cross section. Experimental data points from the H1 experiment [28].

4 Charmonium-nucleon total cross sections

After the light-cone formalism has been checked with the data for virtual photoproduction we are in position to provide reliable predictions for charmonium-nucleon total cross sections. The corresponding expressions are given by Eq. (2)) (compare with [6]). For the GBW and KST dipole cross sections, which have the form $\sigma_0(1 - e^{-r_T^2/r_0^2})$ (see Eqs. (8) and (9)), a summation over spin indexes in (2) gives for the S -states,

$$\mathcal{M}_{\psi p}(s) = \sigma_0 \cdot \left[1 - \pi r_0^2 \int_0^1 d\alpha \int_0^\infty dp_T \int_0^\infty dq_T U(\alpha, p_T) U(\alpha, q_T) V(\alpha, p_T, q_T) \right], \quad (35)$$

where

$$U(\alpha, p_T) = p_T \Phi_\psi(\alpha, p_T) e^{-r_0^2 p_T^2 / 4} \left[(M_1^2(p_T) + p_T^2) (M_2^2(p_T) + p_T^2) \right]^{-1/2}, \quad (36)$$

$$V(\alpha, p_T, q_T) = M_1(p_T)M_1(q_T)M_2(p_T)M_2(q_T) I_0(v) \quad (37)$$

$$+ \left[M_1(p_T)M_1(q_T) + M_1(p_T)M_2(q_T) \right] p_T q_T I_1(v) + p_T^2 q_T^2 I_2(v) ,$$

$$M_1(p_T) = m_c + m_T \sqrt{\frac{\alpha}{1-\alpha}} , \quad (38)$$

$$M_2(p_T) = m_c + m_T \sqrt{\frac{1-\alpha}{\alpha}} , \quad (39)$$

$$v = \frac{1}{2} r_0^2 p_T q_T . \quad (40)$$

Here $m_T^2 = m_c^2 + p_T^2$; $\Phi_\psi(\alpha, p_T)$ is defined in (19); $I_{0,1,2}(v)$ are Bessel functions of imaginary argument.

The calculated J/ψ - and ψ' -nucleon total cross sections are plotted in Fig. 10 for for the GBW and KST forms of the dipole cross sections and all four types of the charmonium potentials.

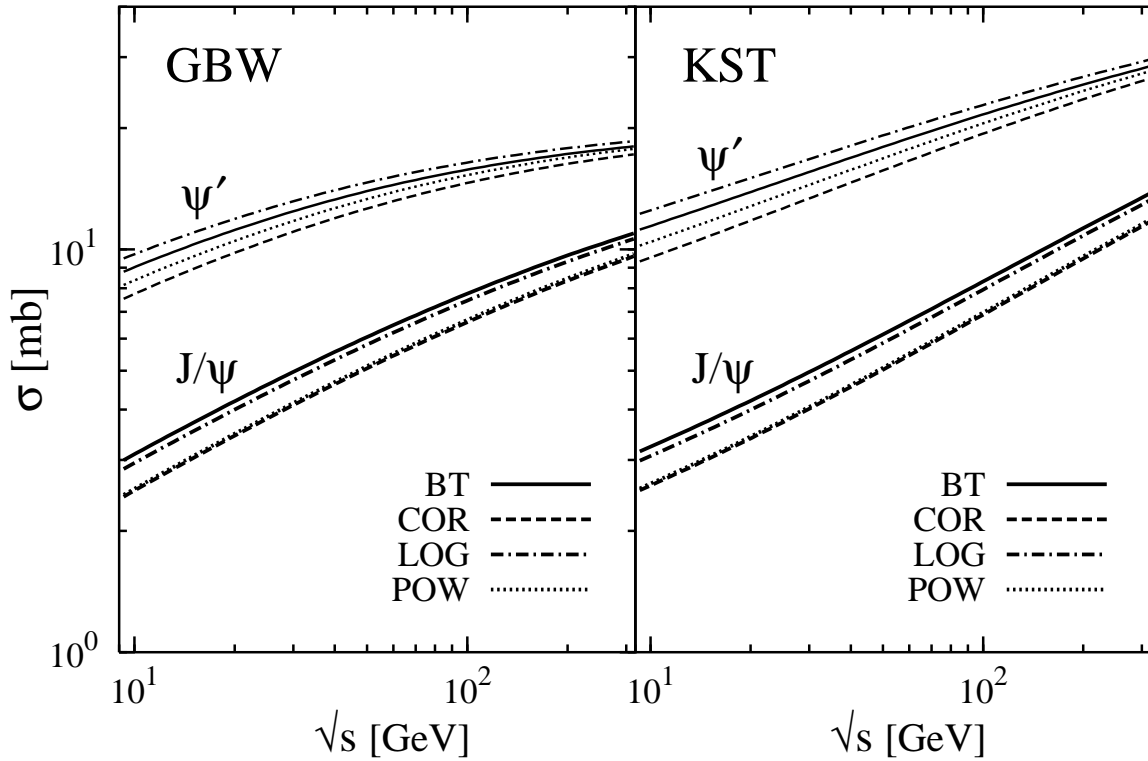


Figure 10: Total $J/\psi p$ (thick curves) and $\psi' p$ (thin curves) cross sections with the GBW and KST parameterizations for the dipole cross section.

The corresponding results for χ -states are depicted in Fig. 11. Here m is the projection

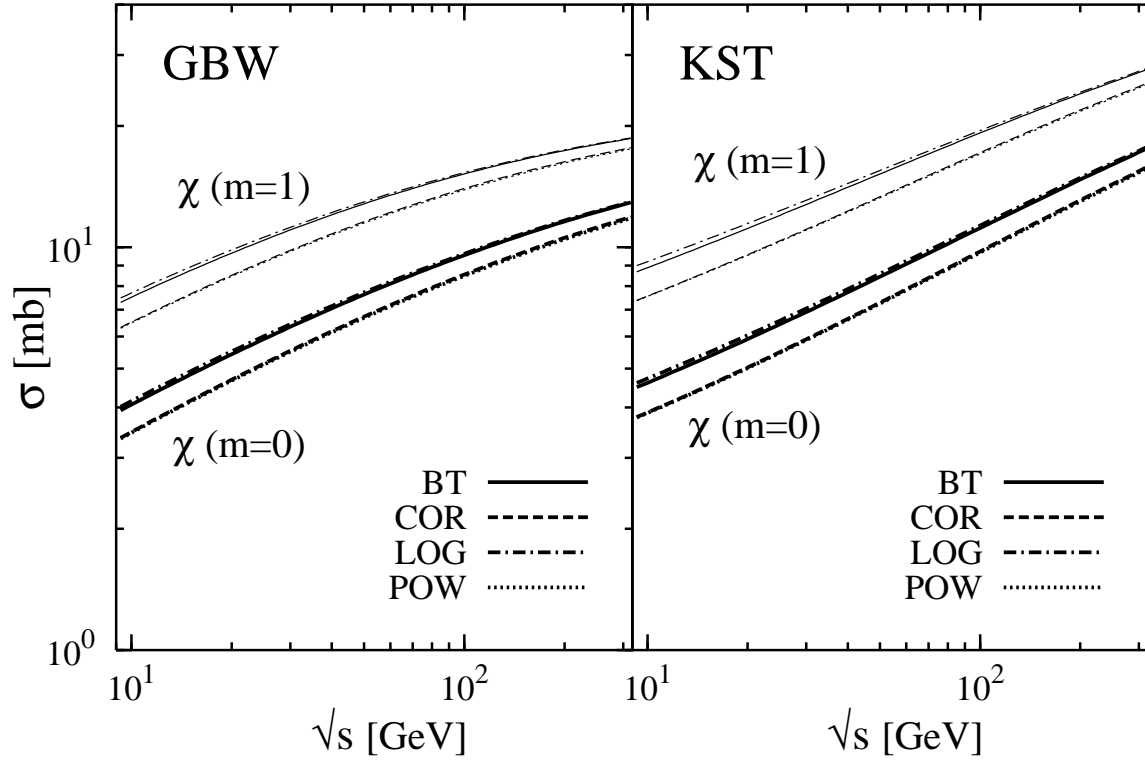


Figure 11: *Total χp ($m = 0$ — thick curves, $m = 1$ — thin curves) cross sections with the KST and GBW parameterizations for the dipole cross section.*

of the orbital momentum which can be zero or one, since this is a P -wave state. From these cross sections with definite m , which we denote σ_m^χ , one can construct the total cross sections for the χ_c states with different spins and helicities λ ,

$$\begin{aligned}
 \chi_{c0}(\lambda = 0) : \quad \sigma &= \frac{1}{3} (2\sigma_1^\chi + \sigma_0^\chi) ; \\
 \chi_{c1}(\lambda = 0) : \quad \sigma &= \sigma_1^\chi ; \\
 \chi_{c1}(\lambda = \pm 1) : \quad \sigma &= \frac{1}{2} (\sigma_1^\chi + \sigma_0^\chi) ; \\
 \chi_{c2}(\lambda = 0) : \quad \sigma &= \frac{1}{3} (\sigma_1^\chi + 2\sigma_0^\chi) ; \\
 \chi_{c2}(\lambda = \pm 1) : \quad \sigma &= \frac{1}{2} (\sigma_1^\chi + \sigma_0^\chi) ; \\
 \chi_{c2}(\lambda = \pm 2) : \quad \sigma &= \sigma_1^\chi .
 \end{aligned} \tag{41}$$

Using these relations one can easily derive the cross sections averaged over helicities which are equal for all three states $\chi_{c0,1,2}$.

The strong dependence of the cross sections for P -wave charmonium states on the projection $m = 0, 1$ of the orbital momentum has been found previously in [40]. However the predicted cross sections at $\sqrt{s} = 10 \text{ GeV}$ for $\chi_c(m = 0)$, $\chi_c(m = 1)$ and ψ' are about twice as large as ours. We believe that the disagreement originates from the too rough nonperturbative dipole cross section¹ used in [40] which was not well adjusted to data. Even the pion-nucleon cross section calculated with Eq. (1) in [40] overestimates the experimental value by factor 1.5.

Although all four potentials are presented, comparison with photoproduction data in Figs. 6 and 7 show that two of them, BT and LOG potentials, are more trustable at least for J/ψ . These two potentials again give very close predictions for J/ψ - p total cross sections but the deviation from the predictions with the two other potentials, COR and POW, is much smaller than in the case of photoproduction.

Note that the cross sections calculated with the GBW parameterization demonstrate a tendency to level off at very high energy, especially for ψ' , as compared to the KST predictions. The reason is obvious: the GBW cross sections approach the universal limit $\sigma_{max} = \sigma_0 = 23.03 \text{ mb}$. This cannot be true, and the KST parameterization is more reliable than GBW at high energies where the gluon cloud surrounding the $\bar{c}c$ pair becomes nearly as big as light hadrons.

According to Figs. 10 and 11 for the KST parameterization the total cross sections of charmonia are nearly straight lines as function of \sqrt{s} in a double logarithmic representation, though with significantly different slopes for the different states. Therefore a parameterization in the form

$$\sigma^{\psi p}(s) = \sigma_0^{\psi} \cdot \left(\frac{s}{s_0}\right)^{\Delta}, \quad (42)$$

¹we are thankful to Lars Gerland who provided us with the expression for the dipole cross section used in [40].

seems appropriate, at least within a restricted energy interval. We use the data shown in Figs. 10 and 11 for the KST parameterization of $\sigma_{q\bar{q}}$ and for the BT and LOG potentials and fit them by the form (42) with $s_0 = 1000 \text{ GeV}$. The two values from the BT and LOG potentials have been averaged and their half difference gives the error estimation. Table 2 shows values for σ_0^ψ and Δ averaged over the energy interval $10 \text{ GeV} < \sqrt{s} < 300 \text{ GeV}$, and the bound state sizes $\langle r_T^2 \rangle$. As expected σ_0^ψ rises monotonically with the size of the

Table 2: *Averaged sizes $\langle r_T^2 \rangle$ for charmonia bound states together with σ_0 and Δ in the parameterization (42) for the J/ψ -, ψ' - and χ -proton cross sections. Estimation of the errors is given in the text.*

	$\langle r_T^2 \rangle [\text{fm}^2]$	$\sigma_0^\psi [\text{mb}]$	Δ
J/ψ	0.117 ± 0.003	5.59 ± 0.13	0.212 ± 0.001
$\chi (m = 0)$	0.181 ± 0.004	7.17 ± 0.07	0.195 ± 0.001
$\chi (m = 1)$	0.362 ± 0.007	13.17 ± 0.16	0.164 ± 0.002
ψ'	0.517 ± 0.034	16.63 ± 0.59	0.139 ± 0.005

charmonium state, and the cross section for $\psi' N$ is about three times larger than for J/ψ . This deviates from the r^2 scaling, since the mean value $\langle r^2 \rangle$ is 4 times larger for ψ' than for J/ψ . The exponent Δ which governs the energy dependence decreases monotonically with the size of the charmonium state, demonstrating the usual correlation between the dipole size and the steepness of energy dependence. The values of Δ are larger than in soft interactions of light hadrons (~ 0.08), but smaller than values reached in DIS at high Q^2 .

Our results at $\sqrt{s} = 10 \text{ GeV}$ (the mean energy of charmonia produced in the NA38/NA50 experiments at SPS, CERN),

$$\sigma_{tot}^{J/\psi}(\sqrt{s} = 10 \text{ GeV}) = 3.56 \pm 0.08 \text{ mb} , \quad (43)$$

$$\sigma_{tot}^{\psi'}(\sqrt{s} = 10 \text{ GeV}) = 12.19 \pm 0.61 \text{ mb} , \quad (44)$$

well agree with the cross sections extracted in [2] from photoproduction data employing the two-channel approximation, $2.8 \pm 0.12 \text{ mb} < \sigma_{tot}^{J/\psi}(\sqrt{s} = 10 \text{ GeV}) < 4.1 \pm 0.15 \text{ mb}$ and $\sigma_{tot}^{\psi'}/\sigma_{tot}^{J/\psi} \approx 3.75$ (having poorly controlled accuracy), which shows that the two channel approach is a reasonable tool to analyze photoproduction data.

The cross section Eq. (42)) with the parameters in Table 2 agrees well with $\sigma_{tot}^{J/\psi}(\sqrt{s} = 20 \text{ GeV}) = 4.4 \pm 0.6 \text{ mb}$ obtained in the model of the stochastic vacuum [41].

It worth noting that the results for charmonium-nucleon total cross sections are amazingly similar to what one could get without any spin rotation,

$$\sigma_{tot}^{\psi N}(s) \approx \int_0^1 d\alpha \int d^2\vec{r}_T |\Phi_\psi(\alpha, \vec{r}_T)|^2 \sigma_{q\bar{q}}(r_T, s), \quad (45)$$

where $\Phi_\psi(\alpha, \vec{r}_T)$ is related by Fourier transformation to Eq. (19), or even performing a simplest integration using the nonrelativistic wave functions (13) in the rest frame of the charmonium:

$$\sigma_{tot}^{\psi N}(s) \approx \int d^3r |\Psi(\vec{r})|^2 \sigma_{q\bar{q}}(r_T, s). \quad (46)$$

The comparison presented in Fig. 12 for the BT potential shows that (45) - (46) are only about 10% below the exact calculation for J/ψ , while there is practically no difference between the exact and approximate calculations for ψ' .

5 Nuclear suppression of charmonium production

Production of charmonia off nuclei seem to be a natural source of information about charmonium-nucleon cross section since nuclear absorption leads to suppression of the production rate measured experimentally. However, one should be cautious applying our results to a calculation of nuclear attenuation of charmonium. In exclusive photoproduction of charmonia the uncertainty principle does not allow to resolve between J/ψ and ψ' unless the formation time, $t_f = 2 E_\psi / (M_{\psi'}^2 - M_{J/\psi}^2)$ [3, 42], is shorter than the mean inter-nucleon separation in nuclei. Only one experiment [43] at $\sim 20 \text{ GeV}$ satisfies this condition. Analyzed with an optical model it leads to $\sigma_{in}^{J/\psi N} = 3.5 \pm 0.8 \text{ mb}$ in a good agreement with our calculations.

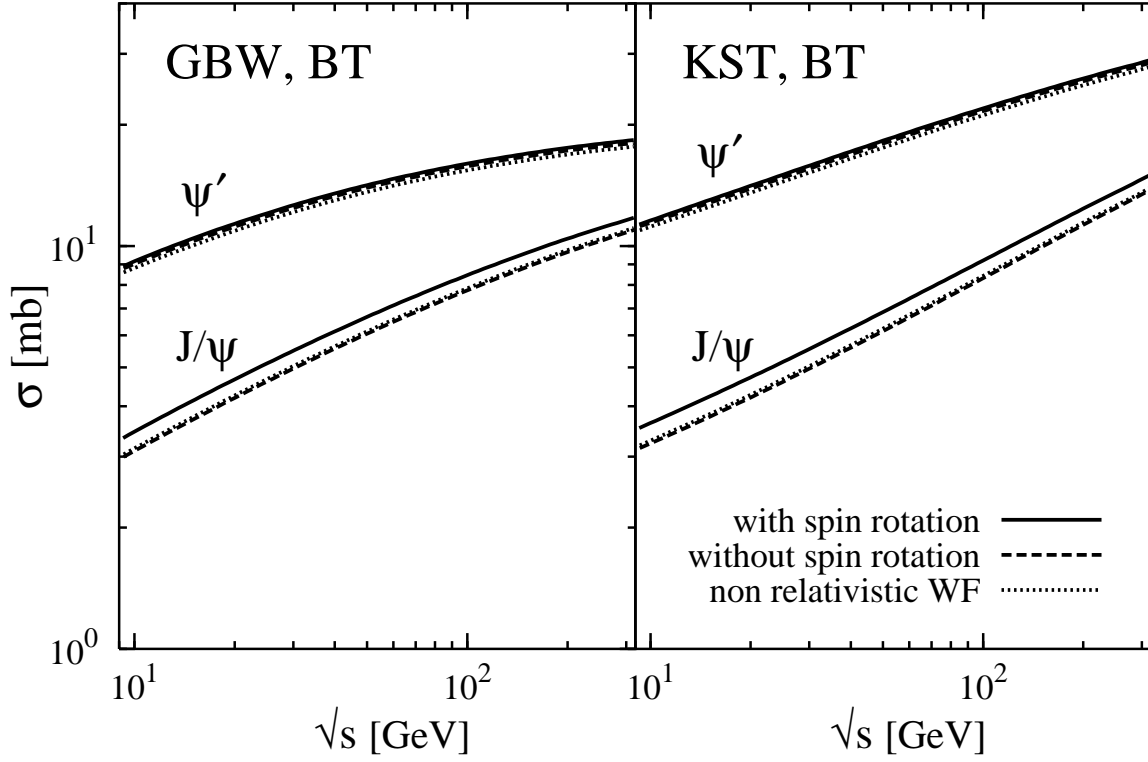


Figure 12: Comparison of the results for $\sigma_{tot}^{\psi N}(s)$ obtained with the exact expression (2) (solid curves) and with the approximations (45) (dashed) and (46) (dotted).

The nuclear photoproduction data [44] taken at 120 GeV cannot be treated in the same way since the formation time, $l_f \approx 10 \text{ fm}$ exceeds the nuclear size. In addition, the coherence length, $l_c = 2 E_\psi / (M_{J/\psi}^2 + Q^2)$ [3, 45], is also long, about 5 fm substantially increasing the attenuation path for the produced $\bar{c}c$ pair.

In the case of hadroproduction of charmonia off nuclei, the interplay of the formation and coherence time effects are as important as in photoproduction. On top of that, the situation is complicated by decays of χ s and ψ' which substantially feed the yield of J/ψ . These heavier states, even if their absorption cross sections are known from our calculations, are also subject to the effects of formation and coherence lengths.

In the analysis [46] of data from the experiment E866 of $pA \rightarrow J/\psi X$ collisions at 800 GeV , proper attention has been given to coherence and formation time effects with the result

(extrapolated to $\sqrt{s} = 10 \text{ GeV}$)

$$\sigma_{eff}^{J/\psi''p} = 5.0 \pm 0.4 \text{ mb} , \quad (47)$$

$$\sigma_{tot}^{\psi'p} = 10.5 \pm 3.6 \text{ mb} , \quad (48)$$

The effective J/ψ -nucleon cross section which is fed by decays of heavier states can be estimated as follows,

$$\frac{1}{\sigma_{eff}} \left(1 - e^{-\sigma_{eff} \langle T \rangle} \right) = \sum_{i=1}^4 \frac{w_i}{\sigma_{tot}^{\psi_i N}} \left(1 - e^{-\sigma_{tot}^{\psi_i N} \langle T \rangle} \right) , \quad (49)$$

where $\langle T \rangle \approx 0.75 \rho_A R_A$ is the mean thickness of a nucleus with radius R_A and the mean density $\rho_A \approx 0.16 \text{ fm}^{-3}$.

Eq. (49) is relevant for J/ψ suppression in nuclear collisions (proton-nucleus and nucleus-nucleus). In this reactions the observed J/ψ arises from directly produced J/ψ 's with probability $w_1 < 1$ and from the other states χ , ψ' via decay after the charmonia have left the interaction zone, where w_i is the probability that the state “i” contributes to the finally observed J/ψ . Values for w_i and $\sigma_{tot}^{\psi_i p}$ are given in Table 3 where $m = 0, 1$ is the projection of the orbital momentum of the $\bar{c}c$ pair on the direction of gluon-gluon collision in $\chi_{1,2}$ production (χ_0 has a tiny branching to J/ψ). It turns out that χ_1 and χ_2 with $m = 0$ cannot be produced or are strongly suppressed in gluon fusion due to the selection rules which forbid projections ± 1 for the total angular momentum (e.g. see [47]), this is why we put $w_2 = 0$.

We calculate σ_{eff} for tungsten used in the analysis [46] and find for $\sqrt{s} = 10 \text{ GeV}$

$$\sigma_{eff}^{J/\psi''p} = 5.8 \pm 0.2 \text{ mb} , \quad (50)$$

where the main uncertainty arises from the w_i . This number is in a good accord with Eq. (47), while the calculated value for $\sigma_{tot}^{\psi'p}$ Eq. (44) agrees well with (48).

The coherence effects are quite important even at the energy of the NA38/NA50 experiments ($E_\psi \approx 50 \text{ GeV}$) at CERN, this is why the effective absorption cross section for ψ' production suggested by the data is about a half of the value we predict. At the energies of RHIC and LHC both the coherence and formation times substantially exceed the sizes of heavy nuclei, and shadowing becomes the dominant phenomenon.

Table 3: Values for the J/ψ -, ψ' -, χ - and effective “ J/ψ ”-proton cross sections at energy $\sqrt{s} = 10 \text{ GeV}$. Errors are given by averaging on BT and LOG potentials for the wave functions.

	w_i	$\sigma [\text{mb}]$
J/ψ	0.52 - 0.6	3.56 ± 0.08
$\chi(m=0)$	0	4.66 ± 0.06
$\chi(m=1)$	0.32 - 0.4	9.05 ± 0.16
ψ'	0.08	12.19 ± 0.61

6 Conclusion and discussions

In this paper we have proposed a simultaneous treatment of elastic photoproduction $\sigma_{\gamma^* p \rightarrow \psi p}(s, Q^2)$ of charmonia and total cross sections $\sigma_{tot}^{\psi p}(s)$. The ingredients are (i) the factorized light-cone expressions (1) - (2) for the cross sections; (ii) the perturbative light-cone wave functions for the $c\bar{c}$ component of the γ^* ; (iii) light cone wave functions for the charmonia bound states, and (iv) a phenomenological dipole cross section $\sigma_{q\bar{q}}(r_T, s)$ for a $c\bar{c}$ interacting with a proton.

The dipole cross section rises with energy; the smaller is the transverse $\bar{q}q$ separation, the steeper is the growth. The source of the energy dependence is the expanding cloud of gluons surrounding the $\bar{q}q$ pair. The gluon bremsstrahlung is more intensive for small dipoles. The gluon cloud can be treated as a joint contribution of higher Fock states, $|\bar{q}q nG\rangle$, however, it can be also included into the energy dependence of $\sigma_{q\bar{q}}(r_T, s)$, as we do, and this is the full description. Addition of any higher Fock state would be the double counting.

As function of energy the initial size of the $\bar{q}q$ source is gradually “forgotten” after multi-step radiation, the small cross sections grow steeper and eventually approach the larger ones at very high energies. All the cross sections are expected to reach a universal asymptotic behavior which saturates the Froissart bound.

The effective dipole cross section $\sigma_{q\bar{q}}(r_T, s)$ is parameterized in a form which satisfies the expectations $\sigma_{q\bar{q}} \propto r_T^2$ for $r_T \rightarrow 0$ (color transparency), but levels off for $r_T \rightarrow \infty$. Two parameterizations for $\sigma_{q\bar{q}}(r_T, s)$, whose form and parameters have been fitted to describe $\sigma_{tot}^{\pi p}(s)$ and the structure function $F_2(x, Q^2)$ are used in our calculations.

While the description of the photon wave function is quite certain, the light-cone wave function of charmonia is rather ambiguous. We have followed the usual recipe in going from a nonrelativistic wave function calculated from a Schrödinger equation to a light cone form. We have included the Melosh spin rotation which is often neglected and found that it is instrumental to obtain agreement, since no parameter is adjustable. In particular, it increases the ψ' photoproduction cross section by a factor 2 - 3 and rises the ψ' to J/ψ ratio to the experimental value.

At the same time, the charmonium-nucleon total cross sections (J/ψ , ψ' , $\chi(m=0)$ and $\chi(m=1)$) turn out to be rather insensitive to the way how the light-cone wave function is formed, even applying no Lorentz transformation one arrives at nearly the same results. This is why we believe that the predicted charmonium-nucleon cross section are very stable against the ambiguities in the light-cone wave function of charmonia. A significant energy dependence is predicted which varies from state to state in accord with our expectations.

We show our predictions for charmonium-nucleon cross sections in a restricted energy range $10 \text{ GeV} < \sqrt{s} < 300 \text{ GeV}$, but this interval can be largely extended in both directions. Since the OZI rule suppresses the leading Reggeons, one can stay with gluonic exchanges rather far down to low energies, unless the charmed Reggeon exchanges become important [48].

Acknowledgment: This work has been supported by a grant from the Gesellschaft für Schwerionenforschung Darmstadt (GSI), grant no. HD HÜFT and by the Federal Ministry BMBF grant no. 06 HD 954, by the grant INTAS-97-OPEN-31696, and by the European Network: Hadronic Physics with Electromagnetic Probes, Contract No. FMRX-CT96-0008

References

- [1] T. Matsui and H. Satz, Phys. Lett. **B178** (1986) 416.
- [2] J. Hüfner and B.Z. Kopeliovich, Phys. Lett. **B426** (1998) 154.
- [3] B.Z. Kopeliovich and B.G. Zakharov, Phys. Rev. **D44** (1991) 3466.
- [4] J.B. Kogut and D.E. Soper, Phys. Rev. **D1** (1970) 2901;
- [5] J.M. Bjorken, J.B. Kogut and D.E. Soper, **D3** (1971) 1382
- [6] A.B. Zamolodchikov, B.Z. Kopeliovich and L.I. Lapidus, JETP Lett. **33** (1981) 595.
- [7] L.N. Lipatov, Sov. Phys. JETP **63** (1986) 904.
- [8] Yu.L. Dokshitzer, V.A. Khoze, A.H. Mueller and S.I. Troyan, “Basics of Perturbative QCD”, Editions Frontieres, ADAGP, Paris 1991.
- [9] B.Z. Kopeliovich, I.K. Potashnikova, B. Povh, E. Predazzi, Phys. Rev. Lett. **85** (2000) 507
- [10] K. Golec-Biernat and M. Wüsthoff, Phys. Rev. **D53** (1999) 014017; hep-ph/9903358.
- [11] B. Kopeliovich, A. Schäfer and A. Tarasov, *Nonperturbative Effects in Gluon Radiation and Photoproduction of Quark Pairs*, to appear in Phys.Rev. **D**; hep-ph/9908245.
- [12] M.G. Ryskin, R.G. Roberts, A.D. Martin and E.M. Levin, Z. Phys. **C76** (1997) 231.
- [13] W. Lucha and F.F. Schöberl, Int.J.Mod.Phys. **C10** (1999) 607-620; hep-ph/9811453.
- [14] W. Buchmüller and S.-H.H. Tye, Phys. Rev. **D24** (1981) 132.
- [15] E. Eichten, K. Gottfried, T. Konoshita, K.D. Lane and T.-M. Yan, Phys. Rev. **D17** (1978) 3090; Phys. Rev. **D21** (1980) 203.
- [16] C. Quigg and J.L. Rosner, Phys.Lett. **B71** (1977) 153.

- [17] A. Martin, Phys.Lett. **B93** (1980) 338.
- [18] O. Benhar, B.Z. Kopeliovich, Ch. Mariotti, N.N. Nikolaev and B.G. Zakharov, Phys. Rev. Lett. **69** (1992) 1156.
- [19] M.V.Terent'ev, Sov.J. Nucl. Phys. **24** (1976) 106.
- [20] P. Hoyer and S. Peigné, Phys. Rev. **D61** (2000) 031501(R)
- [21] K. Suzuki et al., *Validity of the Color Dipole Approximation for Diffractive Production of Heavy Quarkonium*, hep-ph/0005250
- [22] H.J. Melosh, Phys. Rev. **D9** (1974) 1095; W. Jaus, Phys. Rev. **D41** (1990) 3394.
- [23] M.G. Ryskin, Z. Phys. **C37** (1993) 89.
- [24] S.J. Brodsky et al., Phys. Rev. **D50** (1994) 3134; L.L. Frankfurt, W. Koepf and M.I. Strikman, Phys. Rev. **D54** (1996) 3194
- [25] J. Nemchik et al., Z. Phys. **C75** (1997) 71.
- [26] J.B. Bronzan, G.L. Kane and U.P. Sukhatme, Phys.Lett. **B49** (1974) 272.
- [27] H1 Collab., C. Adloff *et al.*, Phys. Lett. **B421** 385 (1998); hep-ex/9711012.
- [28] H1 Collab., C. Adloff *et al.*, Eur. Phys. J. **C10** 373 (1999); hep-ex/9903008.
- [29] H1 Collab., C. Adloff *et al.*, DESY 00-037; hep-ex/0003020.
- [30] ZEUS Collab., J. Breitweg *et al.*, Z. Phys. **C75** 215 (1997).
- [31] ZEUS Collab., J. Breitweg *et al.*, Eur. Phys. J. **C6** 603 (1999).
- [32] E401 Collab., M. Binkley *et al.*, Phys. Rev. Lett. **48** 73 (1982).
- [33] E516 Collab., B. H. Denby *et al.*, Phys. Rev. Lett. **52** 795 (1984).
- [34] U. Camerini *et al.*, Phys. Rev. Lett. **35** 483 (1975).

- [35] NA14 Collab., R. Barate *et al.*, Z. Phys. **C33** 505 (1987).
- [36] E401 Collab., M. Binkley *et al.*, Phys. Rev. Lett. **50** 302 (1983).
- [37] EMC Collab., J.J. Aubert *et al.*, Nucl. Phys. **B213** 1 (1983).
- [38] NMC Collab., P. Amaudraz *et al.*, Nucl. Phys. **B371** 553 (1992).
- [39] J. Hüfner and B.Z. Kopeliovich, Phys. Lett. **B426** (1998) 154.
- [40] L. Gerland, L. Frankfurt, M. Strikman, H. Stcker, W. Greiner, Phys. Rev. Lett. **81** (1998) 762
- [41] H. G. Dosch, F. S. Navarra, M. Nielsen, M. Rueter, Phys. Lett. **B466** (1999) 363; H.G. Dosch, T. Gousset, G. Kulzinger, H.J. Pirner, Phys.Rev. **D55** (1997) 2602
- [42] J. Hüfner and B.Z. Kopeliovich, Phys. Rev. Lett. **76** (1996) 192
- [43] R.L. Anderson *et al.*, Phys. Rev. Lett. **38** (1977) 263.
- [44] M.D. Sokoloff *et al.*, Phys. Rev. Lett. **57** (1986) 3003.
- [45] J. Hüfner, B.Z. Kopeliovich and J. Nemchik, Phys. Lett. **B383** (1996) 362
- [46] Y.B. He, J. Hüfner and B.Z. Kopeliovich, Phys. Lett. **B477** (2000) 93
- [47] M. Vanttinen et al., Phys. Rev. **D51** (1995) 3332
- [48] T. Barnes, E.S. Swanson and C.Y. Wong, *Charmonium + Light Hadron Cross Sections*, nucl-th/0006012